

CFD MODELING OF A SOLITARY WAVE OVERTOPPING BREAKWATER OF VARYING SUBMERGENCE

Mehrdad Bozorgnia¹, Amirhossein Eftekharian², Jiin-Jen Lee³

In this paper, interaction of a nonlinear solitary wave with a submerged breakwater as well as a breakwater with zero freeboard are modeled using Computational Fluid Dynamic (CFD). Simulation results of water particle velocities as well as water surface elevations at the vicinity of breakwater are validated by comparison to experimental data. In order to find out the best turbulence modeling appropriate for wave-breakwater interaction problem, simulations are conducted using standard K-Epsilon, SST-K-Omega, and inviscid models available within the CFD software. In cases involving wave breaking, simulations are also repeated using second order SST-K-Omega model. The overall pattern of the wave interaction with breakwater is adequately reproduced by the CFD software. The processes of wave reflection, wave breaking, and vortical motion at the vicinity of breakwater are correctly captured. The good results achieved are promising regarding the use of CFD for design of breakwaters and other marine structures subject to waves.

Keywords: Wave overtopping; Wave breaking, Vortical motion; Solitary wave; Computational Fluid Dynamic; Turbulence modeling

INTRODUCTION

Interaction of nonlinear waves with marine structures such as breakwaters has been an important problem for coastal and ocean engineers. When the water depth at the breakwater site is close to the breakwater height, and the incident wave amplitude is large, a substantial wave overtopping can be expected. Experiments involving wave overtopping conducted by Zhuang and Lee (1996) showed that the overtopping wave constituted a jet-like water mass impacting the shoreward region of the breakwater. This jet-like water mass induced strong vortices and large water particle velocities in both the horizontal and vertical direction. The large rotational velocity field could remove the armor units of the breakwater and scour the bed. Figure 1 presents a series of four photographs taken during one experimental run for a solitary wave with wave height to water depth ratio of $H/d = 0.3$ (where d was kept constant at $d = 22.86\text{cm}$) overtopping a submerged breakwater. The blue dye was injected in the shoreward region of the breakwater before the wave was generated. The solitary wave propagates from left to right direction in the pictures. The breakwater can be seen at the lower left corner of the pictures. Figure 1 also shows a complete process of vortex generation while solitary wave passes over the submerged breakwater. In this figure, it is observed that a strong rotational flow field has been generated in the vicinity of the shoreward breakwater. In consecutive figures, the vortex was shown to grow bigger and bigger after the wave has passed and eventually move downstream and become disintegrated.

Wave overtopping is a complex physical process and modeling it is challenging since it involves complicated processes such as wave run-up, wave breaking and associated turbulence. The lack of reliable predictive models makes modeling wave-breakwater interaction using CFD very meaningful and worthwhile. Many semi-empirical formulations based on flume and basin experiments have been developed in the past. Such formulae try to consider and parameterize the most relevant variables ruling the process. Most of them are simple expressions describing mean overtopping discharges and are biased towards sloping or vertical seawalls. Examples of available numerical modeling of wave-breakwater interaction in the literature include the work by Zhuang and Lee (1996), who came up with a viscous rotational model for wave overtopping over marine structures by combining potential flow theory and the rotational velocity field generated by the separated flow (vortices) of the overtopping waves as they leave the breakwater site. They compared their simulation results for a solitary wave interacting with a submerged breakwater and found them to be in good agreement with experimental data. Their model however, had the shortcoming of not being able to model wave breaking therefore was not able to model wave-breakwater interactions for the case of a breakwater with zero freeboard depth.

Losada et al. (2008) used the model COBRAS-UC, a new version of the COBRAS (Cornell Breaking Waves and Structures) for the computations of the free surface and pressure time series and spectra under regular and irregular waves. They also used the model to reproduce instantaneous and average wave

¹Sonny Astani Department of Civil and Environmental Engineering, University of Southern California, USA

²Sonny Astani Department of Civil and Environmental Engineering, University of Southern California, USA

³Sonny Astani Department of Civil and Environmental Engineering, University of Southern California, USA

overtopping discharge and compared the simulation results to existing semi-empirical formulae and experimental data. Their simulation results were in good agreement with experimental data.

The present study focuses on the application of CFD to the problem of a solitary wave overtopping a breakwater and the comparison of numerical simulation results to experimental data. The main emphasis of this paper is to compare the performance of the most prevailing turbulence modeling approaches in terms of their capability to capture velocity fields at the vicinity of a submerged breakwater in addition to the capability of the CFD software to capture the water surface profile in wave breaking events induced by zeroing freeboard on top of the breakwater (setting water depth equal to the breakwater height).

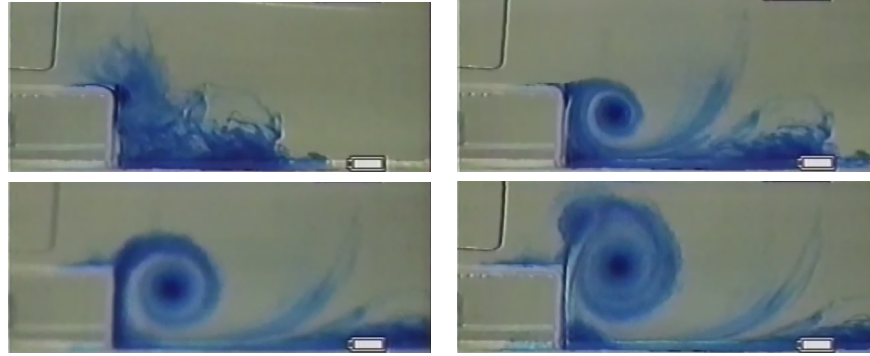


Figure 1: Process of vortex generation while solitary wave passes over the submerged breakwater adapted from Zhuang and Lee (1996).

GOVERNING EQUATIONS

Commercial CFD software STAR-CCM+ from CD-Adapco which works based on three-dimensional two-phase compressible Navier Stokes Equations is used as a tool to compute the wave profile and the velocity field induced by an incoming solitary wave over a submerged breakwater. Previously this software has been used to model interactions of regular waves with bridge superstructures by Bozorgnia and Lee (2013), Bozorgnia and Lee (2012) and Bozorgnia et al. (2011). Relevant equations to be used for wave-breakwater interaction problems are two-dimensional two-phase Navier Stoke (NS) equations. The integral form of NS equations are shown in equations 1 and 2.

$$\frac{d}{dt} \int_V \rho dV + \int_S \rho(\mathbf{v} - \mathbf{v}_g) \cdot d\mathbf{a} = 0 \quad (1)$$

$$\frac{d}{dt} \int_V \rho \mathbf{v} dV + \int_S \rho \mathbf{v} \otimes (\mathbf{v} - \mathbf{v}_g) \cdot d\mathbf{a} = \int_S (\mathbf{T} - p\mathbf{I}) \cdot d\mathbf{a} + \int_V \rho \mathbf{f} dV \quad (2)$$

In these equations ρ is the fluid density, V is the control volume bounded by closed surface S , \mathbf{v} is fluid velocity vector, \mathbf{v}_g is the velocity of Control Volume (CV) surface which is zero in this problem since we do not deal with moving mesh here, t is time, \mathbf{T} is viscous stress tensor and \mathbf{f} is vector of all body forces. Above equations are discretized using Finite Volume Method (FVM) over cells of a computational grid. Discrete versions of the integral form of the Navier-Stokes equations are applied to each control volume. The result is a set of linear algebraic equations with the total number of unknowns in each equation system corresponding to the number of cells in the grid (equation 3).

$$a_p \phi_p^{k+1} + \sum_n a_n \phi_n^{k+1} = b \quad (3)$$

The resulting linear equations are then solved with an algebraic multigrid solver. The coupled system of equations is efficiently solved in a segregated manner, which means that, when solved for each variable, other variables are treated as known. Details about the discretization techniques and segregated flow model used can be found in the large body of work by Ferziger et al. (2002) and STAR CCM+ documentation (CD-adapco (2010)). To capture the interface between air and water in the simulation domain, a variation of the

Volume Of fluid (VOF) method originally proposed by Hirt and Nichols (1981) was used in all simulations. In addition to the conservation equations for mass and momentum, another equation was solved for volume fraction α_i which evolved based on the following transport equation:

$$\frac{d}{dt} \int_V \alpha_i dV + \int_S \alpha_i (v - v_b) \cdot da = 0 \quad (4)$$

where $\alpha_i = \frac{V_i}{V}$ is the volume fraction of the i th phase. In the case of two phase model, in each cell, effective density ρ and molecular viscosity μ are calculated as:

$$\rho = \rho_1 \alpha_1 + \rho_2 \alpha_2 = \rho_1 \alpha_1 + \rho_2 (1 - \alpha_1) \quad (5)$$

$$\mu = \mu_1 \alpha_1 + \mu_2 \alpha_2 = \mu_1 \alpha_1 + \mu_2 (1 - \alpha_1) \quad (6)$$

The discretization of transport equation 4 for α_i requires special care because α_i must be bound between zero and unity and the regions with partially filled cells should be as small as possible (Mozafarjia and Peric (1998)). Three basic turbulence modeling approaches are available: 1-Models that provide closure of the Reynolds-Averaged Navier-Stokes (RANS) equations. 2-Large Eddy Simulation (LES) models and 3-Detached Eddy Simulation (DES) models. Most simulations will rely on the first approach. The second two approaches (LES and DES) are best used after carefully reviewing the applicable literature to gain confidence that the grid resolution requirements can be met and that the computational costs incurred by resolving the small time and length scales are indeed justified. In this paper three turbulence modeling approaches based on closure of Reynolds-Averaged Navier-Stokes (RANS) equations are applied to wave-breakwater interaction problems, and the simulation results are compared with each other with the goal of finding the best turbulence modeling approach applicable to wave-breakwater interaction problems. These turbulence models are standard K-Epsilon, SST-K-Omega and inviscid models. Below these models are briefly explained. More information about these turbulence models including their formulation can be found in CD-adapco (2010).

A standard K-Epsilon turbulence model is a two-equation model in which transport equations are solved for the turbulent kinetic energy k and its dissipation rate ϵ . Various forms of the standard K-Epsilon model have been in use for several decades, and it has become the most widely used model for industrial applications. Since the inception of the standard K-Epsilon model, there have been countless attempts to improve it. The most significant of these improvements have been incorporated into the CFD software. The Standard K-Epsilon Model is a de facto standard version of the two-equation model that involves transport equations for the turbulent kinetic energy and its dissipation rate. The transport equations are of the form suggested by Jones and Launder (1972), with coefficients suggested by Launder and Sharma (1974). Some additional terms have been added to the model in the CFD software to account for effects such as buoyancy and compressibility.

The SST-K-Omega model is another two-equation model that is an alternative to the standard K-Epsilon model. The transport equations solved are for the turbulent kinetic energy k and a quantity called ω , which is defined as the specific dissipation rate, that is, the dissipation rate per unit turbulent kinetic energy. One reported advantage of the SST-K-Omega model over the standard K-Epsilon model is its improved performance for boundary layers under adverse pressure gradients. Perhaps the most significant advantage, however, is that it may be applied throughout the boundary layer, including the viscous-dominated region, without further modification. Furthermore, the standard SST-K-Omega model can be used in this mode without requiring the computation of wall distance. The biggest disadvantage of the SST-K-Omega model, in its original form, is that boundary layer computations are very sensitive to the values of ω in the free stream. This translates into extreme sensitivity to inlet boundary conditions for internal flows, a problem that does not exist for the standard K-Epsilon models. SST-K-Omega Model used in this paper effectively blends a standard K-Epsilon model in the far-field with a SST-K-Omega model near the wall in an attempt to cure the biggest mentioned drawback of SST-K-Omega model for practical flow simulations.

The inviscid model is an idealization resulting from neglecting the viscous effects in simulating the equations of motion. The solution of the resulting Euler equations (as opposed to the Navier-Stokes equations) generally results in significant savings of computer resources, since boundary layers and other viscous effects no longer have to be resolved. Application of each of these turbulence closure models depends on the problem at hand and the significance of each of the physics involved in the problem.

CFD SOFTWARE SETUP & VALIDATION

Building the CFD model involves selecting the mesh resolution, the simulation algorithm, the boundary conditions, including air-water interface properties, and the turbulence model. In addition, in transient simulations, convergence criteria need to be set to make sure simulation results converge at each time step before going to the next time step. In order to validate the capability of the CFD software for generating solitary waves that resemble the ones generated in the experiment, propagation of a solitary wave is modeled by the CFD software and simulation results are compared with LDV measurements in experiment. Boussinesq approximation was used for generating the solitary wave profile which calculates wave profile and horizontal and vertical water particle velocity magnitudes using the below formulas:

1. Wave profile:

$$h(x, t) = H \left[\operatorname{sech} \left(\sqrt{\frac{3H}{4d}} \frac{X}{d} \right) \right]^2 \quad (7)$$

where $X = x - ct$

2. Wave speed:

$$c = \sqrt{g(d + H)} \quad (8)$$

3. Fluid particle velocities:

$$\frac{u}{\sqrt{gd}} = \frac{h}{d} \left\{ 1 - \frac{h}{4d} + \frac{d}{3} \left(\frac{d}{h} \right) \left[1 - \frac{3}{2} \left(\frac{y}{d} \right)^2 \right] \frac{d^2 h}{dx^2} \right\} \quad (9)$$

$$\frac{v}{\sqrt{gd}} = -\frac{y}{d} \left\{ \left(1 - \frac{1}{2} \frac{h}{d} \right) \frac{dh}{dx} + \frac{d^2}{3} \left(1 - \frac{1}{2} \frac{y^2}{d^2} \right) \frac{d^3 h}{dx^3} \right\} \quad (10)$$

Where H is the maximum wave height, d is the water depth, and u and v are horizontal and vertical water particle velocities. Based on the theoretical expressions summarized above, a solitary wave is completely defined for a given water depth d and its crest amplitude H . A solitary wave with a wave height to water depth ratio of $H/d = 0.3$ is generated in a constant water depth of $d = 22.86\text{cm}$. Horizontal and vertical water particle velocities are calculated at a depth of $y/d = -0.825$ (where y is measured from undisturbed free surface) and are compared to the experimental data of Zhuang and Lee (1996). Figure 2 shows a comparison of horizontal and vertical water particle velocities to the experimental data. From figure 2, it can be seen that the water particle velocities of the solitary wave generated using Boussinesq approximation and the CFD software are in good agreement with the experimental data therefore, CFD software can be confidently applied to the wave-breakwater interaction problem. The ordinates in both figures are the velocity components normalized with respect to \sqrt{gd} (the wave celerity in water depth d) and the abscissa is the real time normalized as $t\sqrt{g/d}$.

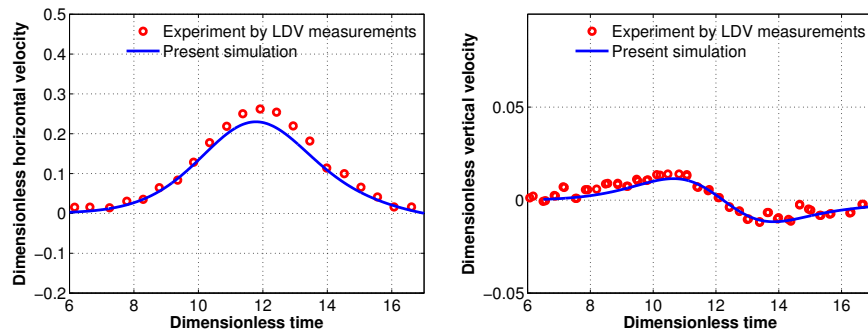


Figure 2: Comparison of horizontal and vertical velocities at $y/d = -0.825$ for $H/d = 0.3$ and $d = 22.86\text{cm}$.

CFD MODELING OF THE INTERACTION OF A SOLITARY WAVE WITH A SUBMERGED RECTANGULAR BREAKWATER

Experiments involving the propagation of solitary waves over various submerged breakwater configurations were conducted by Zhuang and Lee (1996) in a wave tank 15.2 meter long, 39.4 centimeter wide, and 61 centimeter deep. A programmable piston-type wave generator was installed at one end of the tank and a sloping beach was installed at the other end of the tank to aid wave dissipation for the purpose of reducing the waiting time between experimental runs. The water particle velocities were measured using a portable four-beam, two-component, fiber optic Laser Doppler Velocimeter (LDV). Titanium Dioxide powder was used in the experiments as a seeding agent. Figure 3 shows locations where LDV measurements were conducted in the experiment.

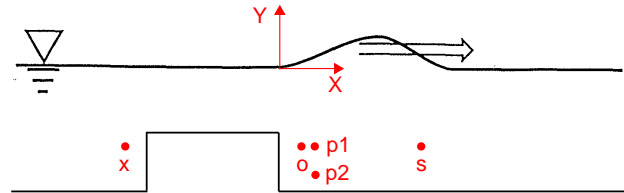


Figure 3: Location of LDV measurements for $H/d=0.3$ and $d=22.86\text{cm}$ for break water A (adapted from Zhuang and Lee (1996)).

The CFD software was configured for modeling the interaction of a solitary wave with a wave height to water depth ratio of $H/d=0.3$ with a submerged rectangular breakwater with the exact dimensions of what was used in experiments conducted by Zhuang and Lee (1996). In all simulations in this section, water depth d was kept constant at 22.86 cm. Horizontal and vertical velocity magnitudes were calculated at various points before and after the submerged breakwater shown in figure 3 and table 1, and the results were compared to experimental data.

Table 1: Locations of water particle velocity measurements within simulation domain (breakwater A).

Point	x/d	y/d
x	-0.1	-0.75
o	0.1	-0.75
p1	0.15	-0.75
p2	0.15	-0.825
s	0.6	-0.75

Figure 4 shows the mesh used in the simulation domain. In order to save on the computational time and number of mesh cells used in the simulation domain, simulation domain was divided into three distinct mesh regions: region 3 contained the finest mesh within the simulation domain and was where the wave-breakwater interaction took place. The mesh used in this region had cell sizes of $\Delta x = \Delta y = 1.25\text{ mm}$. Region 2 was where solitary wave propagation took place within the still water before and after the submerged breakwater. It contained hexahedral mesh cells with sizes of $\Delta x = 5\text{ mm}$ and $\Delta y = 2.5\text{ mm}$. Region 1 contained the coarsest mesh of the simulation domain. Contrary to the other mesh regions, which contained mesh cells of constant size, this region contained mesh cells which varied in size within region 1. The mesh in region 1 was finest close to the mesh in region 2 and coarsest close to the top boundary.

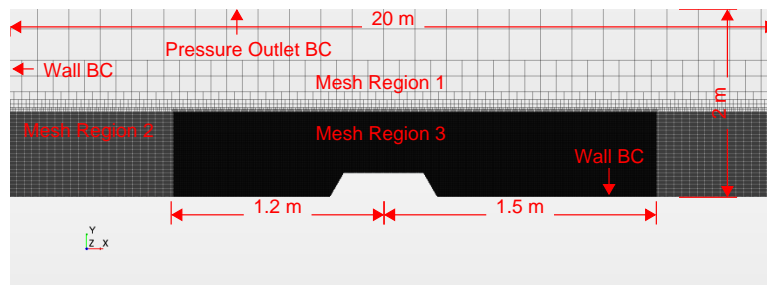


Figure 4: Meshed Simulation domain along with boundary conditions.

The choice of time-step in CFD simulations is an engineering judgment (just like grid refinement) and is related to the time scales of the physical phenomenon under investigation. After conducting several simulations with various time step sizes, a time step size of $\Delta t = 0.001s$ was chosen to ensure solution accuracy and convergence. The wall boundary condition was used everywhere within the simulation domain except for the top boundary, where pressure outlet was specified as a boundary condition (these boundary conditions are shown in figure 4). A wall boundary represents an impermeable surface, an impenetrable boundary for inviscid flows an impenetrable, no-slip boundary for viscous flow simulations. A pressure outlet boundary is a flow outlet boundary at which the pressure is specified. At the top pressure outlet boundary, atmospheric pressure was specified. In order to investigate the influence of turbulence closure models on the CFD simulation results, all simulations of wave-breakwater interactions in this section were conducted using the SST-K-Omega, standard K-Epsilon and inviscid models briefly explained in the previous section and simulation results are compared to experimental. Comparison of horizontal and vertical velocity magnitudes to the experimental data are shown in figures 5 and 6 for points x,o, p1,p2,s.

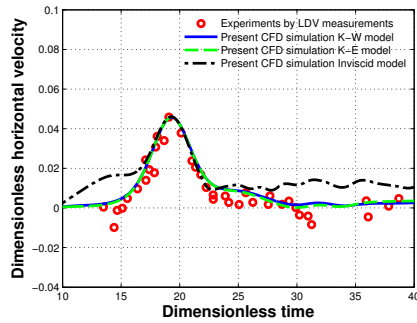
Comparisons of the CFD simulation results to the experimental data at point x 0.1d from the breakwater seaward edge and -0.75d from the still water surface are shown in figures 5(a) and 5(b). As is evident in this figure, both standard K-Epsilon and SST-K-Omega models give identical results which match the experimental data at this point. The inviscid model gives identical results to the standard K-Epsilon and SST-K-Omega models for vertical velocity but slightly deviates from the experimental and standard K-Epsilon and SST-K-Omega model simulation results for horizontal velocity.

Velocity time histories at point o are shown in figures 5(c) and 5(d). Point o is located at 0.1d from the breakwater shoreward edge and -0.75d from the still water surface. Again, standard K-Epsilon and SST-K-Omega models reveal identical results for both horizontal and vertical velocity magnitudes, while the inviscid model results differ slightly from standard K-Epsilon and SST-K-Omega model simulation results and the experimental data for horizontal water particle velocity.

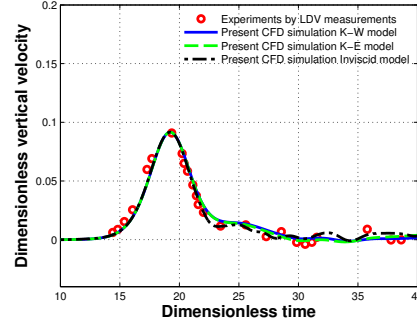
Horizontal and vertical velocity time history comparisons between the present model and the experimental data at location p1 are shown in figure 5(e) and 5(f). Location p1 is -0.75d from the still water surface and 0.15d from the breakwater shoreward surface. It is 0.075d above location p2. As observed in figures 5(e) and 5(f), velocity at location p1 shows the reversal of horizontal velocity from shoreward to seaward direction and the reversal of vertical velocity from downward to upward. Although location p1 is very close to location p2, comparing water particle velocities at locations p1 and p2, we can see the velocity time histories from the two locations have significant differences. This difference in velocity time histories indicates that there is a rapidly changing velocity field in this region, and the vertical velocity reached the maximum when the horizontal velocity became small, indicating location p1 is in the middle left portion of the clockwise rotating vortex, where the flow is basically going up. Simulation results of SST-K-Omega, standard K-Epsilon and inviscid models are very close to each other until non-dimensional time of 17 for horizontal velocity. After this point, both standard K-Epsilon and SST-K-Omega models perform better in predicting the magnitude of horizontal velocity than the inviscid model. SST-K-Omega, standard K-Epsilon and inviscid model results at point p1 seem to overlap each other for vertical velocity at point p1.

Velocity time history at point p2 is shown in figures 6(a) and 6(b). Point p2 is at the vertical position - 0.825d from the still water surface and 0.15d from the breakwater shoreward surface. Examining horizontal and vertical velocities at this point shows that both the CFD simulation results and experimental data show a change in the direction of water particle velocities at this point. The horizontal velocity changes direction from positive to negative and the vertical velocity changes direction from negative to positive. This means

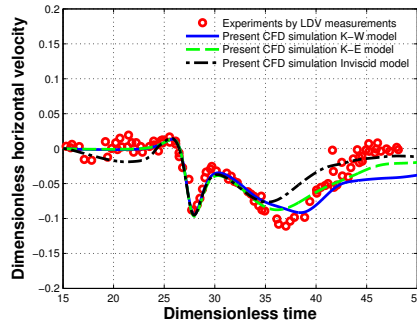
the flow direction at this point changes from forward and downward to backward (seaward) and upward. It clearly shows that a vortical motion has been generated during the wave overtopping process. Another noticeable feature to be observed from this time history graph is the magnitudes of the positive vertical velocity and negative horizontal velocity, which are both much greater than the particle velocities associated with an unmodified solitary wave, which are observed at point x shown in figures 5(a) and 5(b).



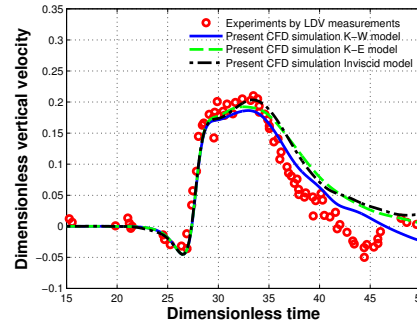
(a) Horizontal velocity magnitude at point x



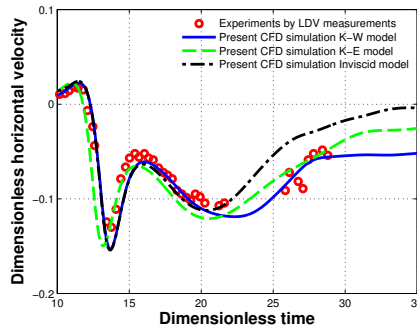
(b) Vertical velocity magnitude at point x



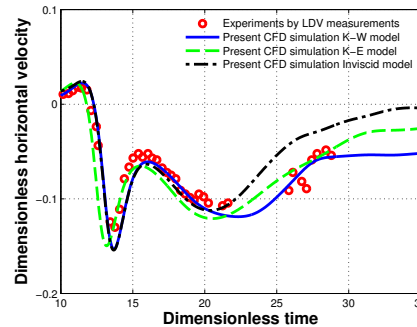
(c) Horizontal velocity magnitude at point o



(d) Vertical velocity magnitude at point o



(e) Horizontal velocity magnitude at point $p1$



(f) Vertical velocity magnitude at point $p1$

Figure 5: Comparison of horizontal and vertical velocity magnitudes at points x , o and $p1$ simulated using $k - \omega$, $k - \epsilon$ and inviscid models to the experimental data for $H/d = 0.3$ and $d = 22.86\text{cm}$.

This feature of increased particle motion could contribute to the destabilization of the breakwater armor units in the shoreward face. Similar to point $p1$, at point $p2$, standard K-Epsilon and SST-K-Omega models show identical horizontal velocity results to inviscid model simulation results till non-dimensional time of 17. After this point SST-K-Omega, standard K-Epsilon, and inviscid models show slightly different results. The SST-K-Omega model seems to do a better job of capturing minimum velocity at this point while the standard K-Epsilon model seems to do better in capturing data points on the upward portion of the velocity graph. The inviscid model seem to have some difficulty capturing data points on the upward portion of the

horizontal water particle velocity plot after non-dimensional time of 17. Not only did it not capture the minimum horizontal velocity at this point, but also it did not capture the data points on upward portion of the velocity graph time history. Likewise, standard K-Epsilon, SST-K-Omega and inviscid models show similar results for vertical velocity until non-dimensional time of 17. After this point, all three models did not do a good job of capturing the magnitude of vertical velocity, although the standard K-Epsilon and inviscid model results seem to be closer to experimental data than SST-K-Omega model simulation results.

Horizontal and vertical velocity time history comparisons between the present model and the experimental data at point s are shown in figures 6(c) and 6(d). Location s is $-0.75d$ from the still water surface and $0.6d$ from the breakwater shoreward surface. At this point, all three models do an excellent job of predicting both horizontal and vertical velocity magnitudes.

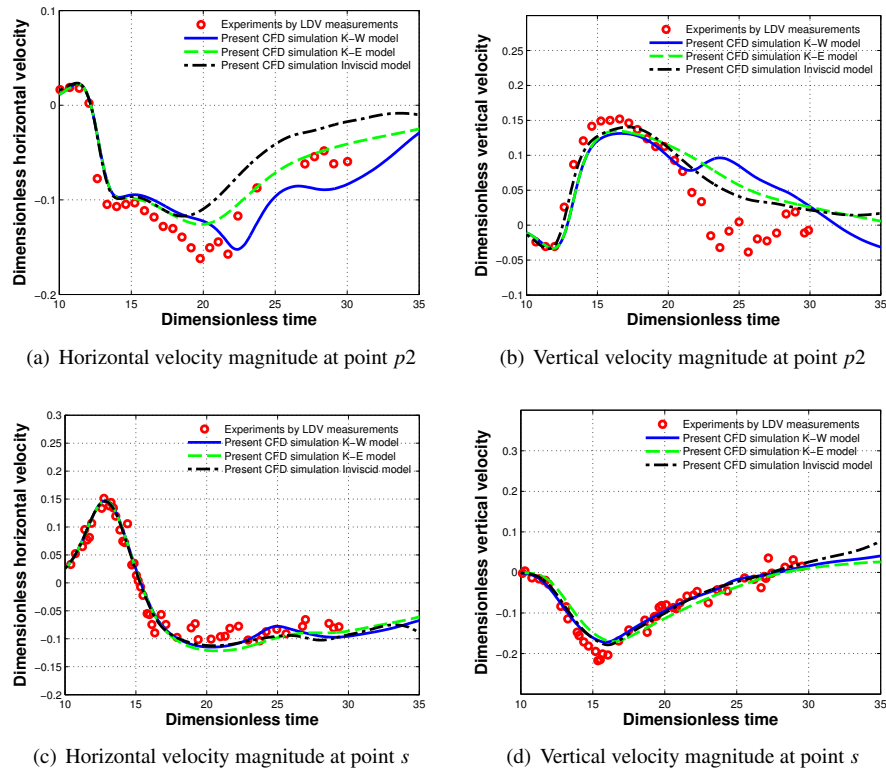


Figure 6: Comparison of horizontal and vertical velocity magnitudes at points $p2$ and s simulated using $k - \omega$, $k - \epsilon$ and inviscid models to the experimental data for $H/d=0.3$ and $d=22.86\text{cm}$.

Overall, the CFD software was able to predict velocity magnitudes in the vicinity of submerged breakwater with very good accuracy. CFD seems to predict the magnitude of vertical velocities with better accuracy compared to horizontal velocities at most points in the vicinity of submerged breakwater. Except for a few specific points, the results of all three turbulence models were very close to each other. SST-K-Omega and standard K-Epsilon models seem to do a better job of predicting horizontal and vertical water particle velocity magnitudes compared to the inviscid model. Even though the SST-K-Omega model is more sophisticated than the standard K-Epsilon model, the standard K-Epsilon model seems to perform slightly better than the SST-K-Omega model in terms of predicting the magnitude of both horizontal and vertical velocities at various points in the vicinity of submerged breakwater. It is worth mentioning that the superiority of the standard K-Epsilon model to the SST-K-Omega model is only investigated for the specific problem of wave-breakwater interaction. In addition, the recommended expert parameters within the CFD software were not changed from the default values. There might be some room to improve the simulation results by changing these parameters which was not investigated in this paper.

CFD MODELING OF A SOLITARY WAVE INTERACTING WITH A TRAPEZOIDAL BREAKWATER WITH ZERO FREEBOARD

In order to investigate the capability of the CFD software in predicting the water surface profile in wave breaking events, extreme wave breaking was introduced into the model by zeroing freeboard on top of breakwater B, (shown in figure 8) and the CFD simulation results were compared to the experimental data. Figure 7 shows a 0.4 solitary wave overtopping on breakwater B in the zero free board situation. With the blue dye, it is clearly seen that a vortex is formed immediately after the wave passed the shoreward breakwater edge. It can also be seen that there is significant amount of air (the white bubbles on the picture) that is entrained into the flow rotation, creating more violent flow motion in the shoreward region of the breakwater. The rapid changing flow field in the shoreward breakwater region under severe wave overtopping conditions may also cause significant bottom scouring. Zhuang and Lee (1996) conducted experiments in which fine sand was placed on the shoreward side of the breakwater in still water conditions before the incident solitary wave was generated. The sand placed at the bottom of the wave tank was shown to have got stirred up by the flow. Eventually the violent flow region moved towards the shoreward face of the breakwater. This phenomenon could aggravate the instability problems for the breakwater armor units and is clearly shown by the large velocity vectors in the computed velocity vector plot shown in figure 11.

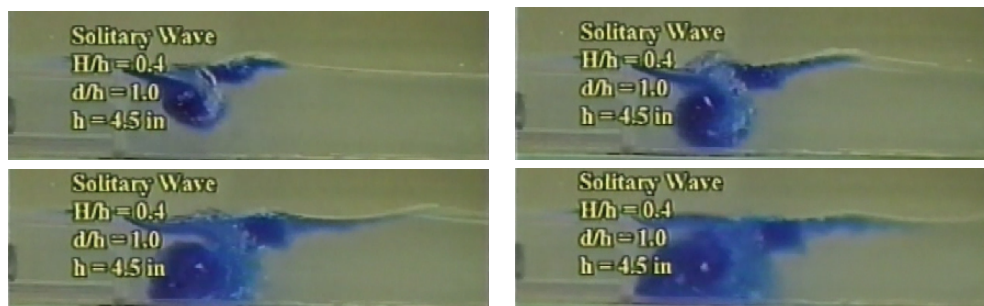


Figure 7: Observations of scouring effect and vortex generation in the shoreward region of breakwater B under solitary wave overtopping.

Obviously, the CFD simulation of wave-breakwater interactions is more challenging for this case because of more violent flow motion and the significant amount of air entrapment and entrainment involved. Simulations were first conducted using the first order standard K-Epsilon and SST-K-Omega models explained in the previous section. Next, in order to improve the accuracy of the simulation results, they were repeated using the second order SST-K-Omega model available within the CFD software, and the results were compared with the first order SST-K-Omega model and experimental data by Zhuang and Lee (1996). Figure 8 shows the geometry of trapezoidal breakwater B (base of 51.26cm, a top of 38.1 cm and a height of 11.43 cm) and locations where water surface elevations were measured (points A, B, and C). In addition to water surface elevation, horizontal and vertical velocity magnitudes were also measured at points E and F located at $2.22d$ from the center of breakwater B and $-0.1d$ and $-0.5d$ from the undisturbed water surface (where d was kept constant at 11.43 cm in all simulations in this section) respectively. The incident solitary wave used in this experiment had an amplitude to depth ratio (H/d) of 0.2. The simulation domain was meshed in a manner identical to the meshed simulation domain shown in figure 4. When an incident solitary wave strikes the breakwater from the left, the overtopping wave propagates over the breakwater at zero water depth until it passes toward the shoreward side of the breakwater. Figure 9(a) is the wave record 114.3 cm (ten water depth) upstream of the center of the breakwater. From figure 9(a) it is clear that the majority of the first wave represents the incident solitary wave and the second wave represents the reflected wave from the upstream edge of the breakwater. The shape of the reflected wave is also quite similar to the solitary wave profile. Looking at figure 9(a), it is evident that the standard K-Epsilon and SST-K-Omega models both do a good job of predicting the incident and reflected wave. The results of the standard K-Epsilon and SST-K-Omega models overlap each other and the experimental data. Figure 9(b) shows the comparison between the first and second order SST-K-Omega models and the experimental data. Again, the second order SST-K-Omega model results seem to overlap the first order SST-K-Omega model

and experimental data.

The wave profile shown in figure 9(c) represents the transmitted wave profile at 38.1 cm downstream (3.33 water depth) after the solitary wave has traveled above the breakwater crest region. It shows that the primary wave is followed by a series of oscillatory tails. These oscillatory wave trains have been reformed into more regular oscillatory waves as they traveled further downstream, as evidenced in the wave profile taken at a location 10 water depth downstream, which is presented in figure 9(e). Looking at figure 9(c), it is evident that the standard K-Epsilon and SST-K-Omega models both do a good job of predicting the peak water elevation but fail to predict oscillatory wave trains following the peak oscillatory wave train. The standard K-Epsilon model seems to perform slightly better than the SST-K-Omega model in predicting the oscillatory wave train, but they both fail to predict negative values with reasonable accuracy (negative values refer to water surface elevations below the undisturbed water surface elevation).

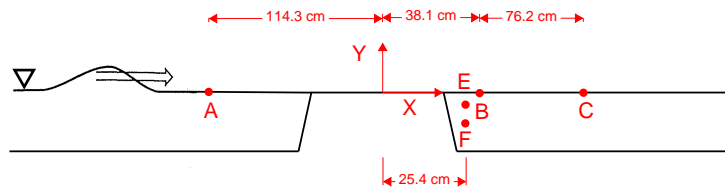


Figure 8: Location of water surface profile and LDV measurements for $H/d=0.3$ and $d=22.86\text{cm}$ for breakwater B (adapted from Zhuang and Lee (1996)).

Figure 9(d) shows comparison between the first and second order SST-K-Omega models and the experimental data. The second order SST-K-Omega model seems to perform slightly better than the first order SST-K-Omega model, especially in capturing negative water surface elevations. However still they both are not able to capture this oscillatory wave train with reasonable accuracy, and the second order SST-K-Omega model also seems to slightly overpredict the magnitude of the peak water elevation.

Figure 9(e) shows the transmitted wave 10 water depth downstream of breakwater. It is interesting to observe the physical nature of the transmitted wave as it travels above the breakwater crest at zero depth. The jet-like water mass is translated into the shoreward region of the breakwater. This water mass which is above the still water level then plunges into the shoreward region by the continuous effect of the gravity forces, causing the water mass in the shoreward region to exhibit significant undulations. Comparing the wave profiles shown in figures 9(a), 9(c) and 9(e), it is clear that the breakwater serves to break up the incident wave, resulting in significant higher frequency wave components in the shoreward region. This phenomenon could significantly influence the basin response of the coastal region by generating higher frequency waves toward the shoreward region. If the shoreward region is connected to a harbor, then the basin response could be significantly altered. The importance of this has been noted by Raichlen et al. (1992). Looking into figure 9(e), it is obvious that both the standard K-Epsilon and SST-K-Omega models underpredict the magnitude of the peak water surface elevation, and they also fail to predict the oscillatory wave train following the peak water surface elevation with reasonable accuracy. The standard K-Epsilon model seems to do a better job of predicting the peak positive values compared to the SST-K-Omega model. Figure 9(f) shows the comparison of the first order SST-K-Omega model to the second order SST-K-Omega model. As is evident in this figure, the second order SST-K-Omega model performs significantly better in predicting both negative and positive peak water elevations in the oscillatory wave train. Not only does it predict the peak values with better accuracy, but it also predicts the oscillatory wave train's period with better accuracy.

Figures 10(a) and 10(b) present horizontal and vertical components of the water particle velocity at location E ($x = 2.22d$, $y = -0.1d$) obtained by LDV measurements. Looking at figure 10(a) we can see that the horizontal water particle velocity is almost equal to the wave celerity. The horizontal water particle velocity under an undisturbed solitary wave with 0.2 amplitude ratio at the location of $0.1d$ below the still water level is approximately $0.2\sqrt{gd}$. Therefore, this is more than four times the water particle velocity at the similar location within the incident wave before the incident wave strikes the breakwater. The relatively large negative vertical component of velocity can also be seen in figure 10(b) showing tremendous impact

of the overtopping waves. Such large water particle velocity of the overtopping wave can cause significant damage if it strikes any marine structure in the passageway of the wave.

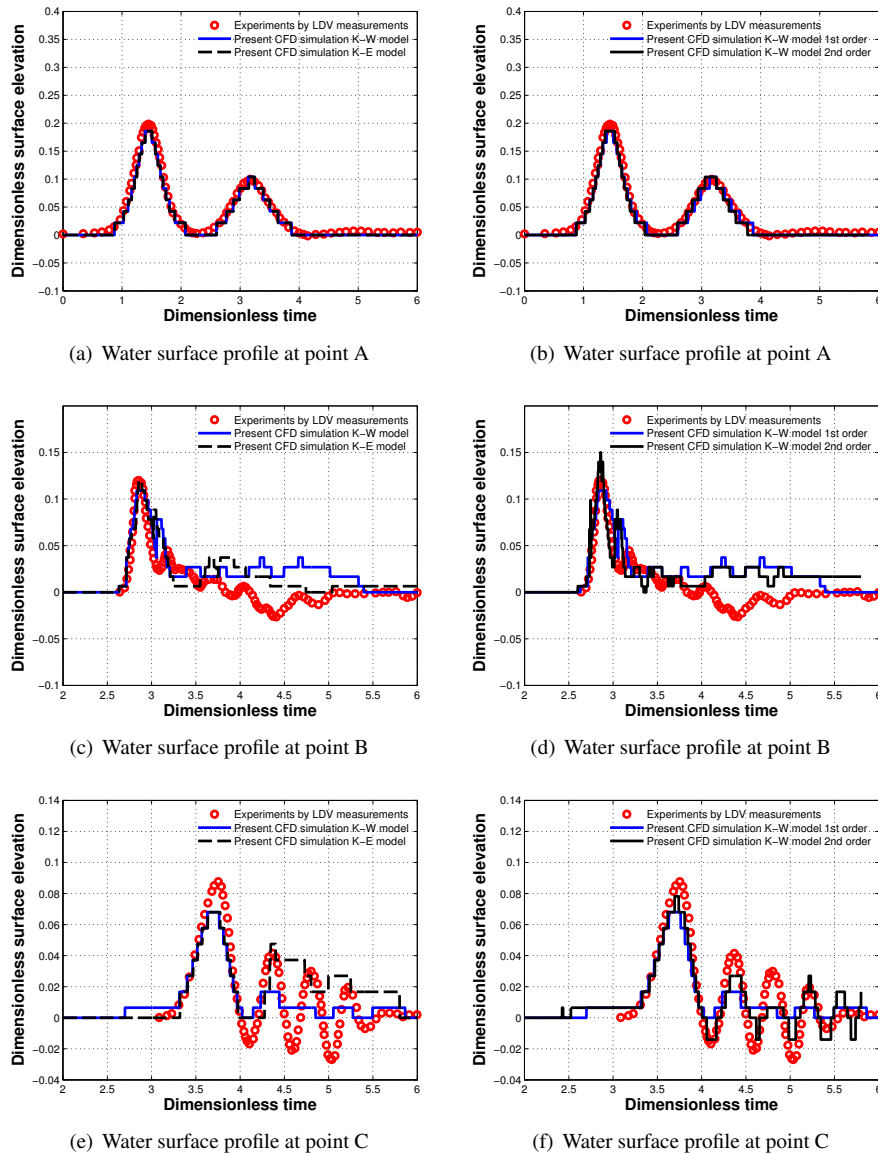
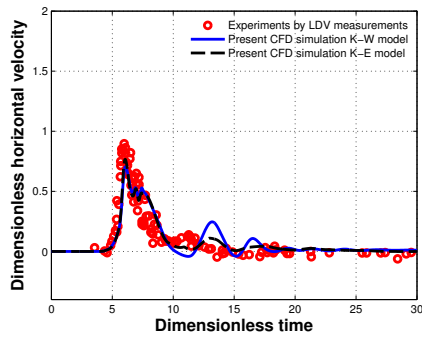
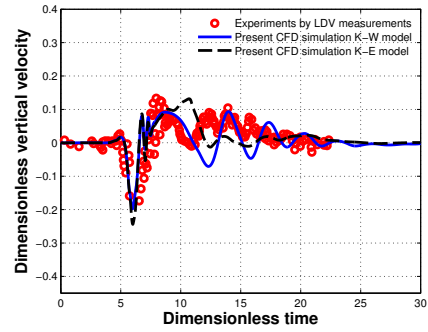


Figure 9: Plots (a), (c), and (e) show comparison of simulated water surface profile using $k - \omega$ and $k - \varepsilon$ turbulence closure models at points A, B, and C to experimental data. Plots (b), (d), and (f) show comparison of simulated water surface profile using $k - \omega$ 1st order and $k - \omega$ 2nd order turbulence closure models at points A, B, and C to experimental data.

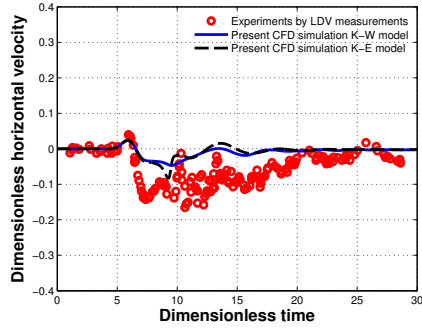
Examining the experimental data of water particle velocities at points E and F shows that the quality of the experimental data at these two points is not as good as the experimental data for the submerged breakwater case. This is likely due to the difficulty of the LDV measurement device in capturing the exact values of water particle velocities in the presence of a significant amount of air entrapment and entrainment in the experiment. From figures 10(a) and 10(b) it can be seen that both standard K-Epsilon and SST-K-Omega models predict the peak horizontal and vertical velocities at point E with reasonable accuracy. However they seem to have difficulty predicting the horizontal and vertical water particle velocities after the peak point.



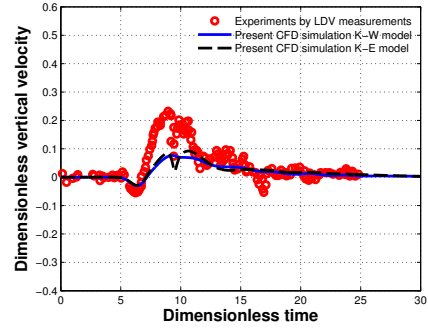
(a) Horizontal velocity at point E



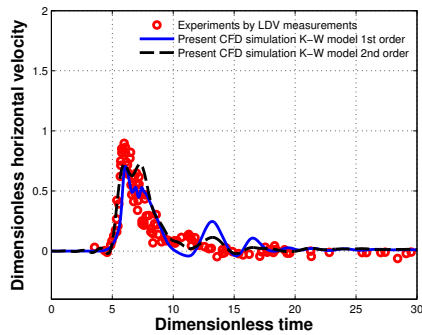
(b) Vertical velocity at point E



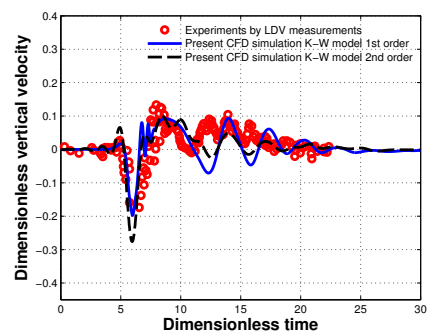
(c) Horizontal velocity at point F



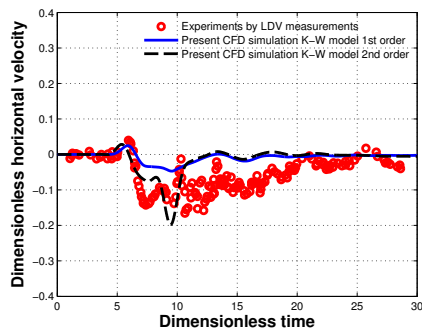
(d) Vertical velocity at point F



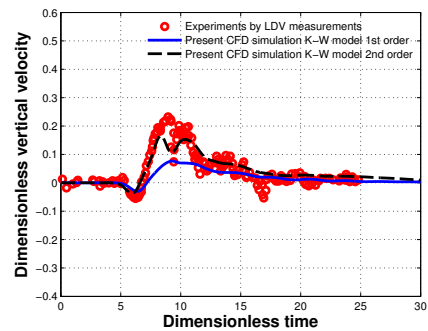
(e) Horizontal velocity at point E



(f) Vertical velocity at point E



(g) Horizontal velocity at point F



(h) Vertical velocity at point F

Figure 10: Plots (a), (b), (c), and (d) show comparison of simulated water particle velocities using $k - \omega$ and $k - \epsilon$ turbulence closure models at points E and F to experimental data. Plots (e), (f), (g), and (h) show comparison of simulated water particle velocities using $k - \omega$ 1st order and $k - \omega$ 2nd order turbulence closure models at points E and F to experimental data.

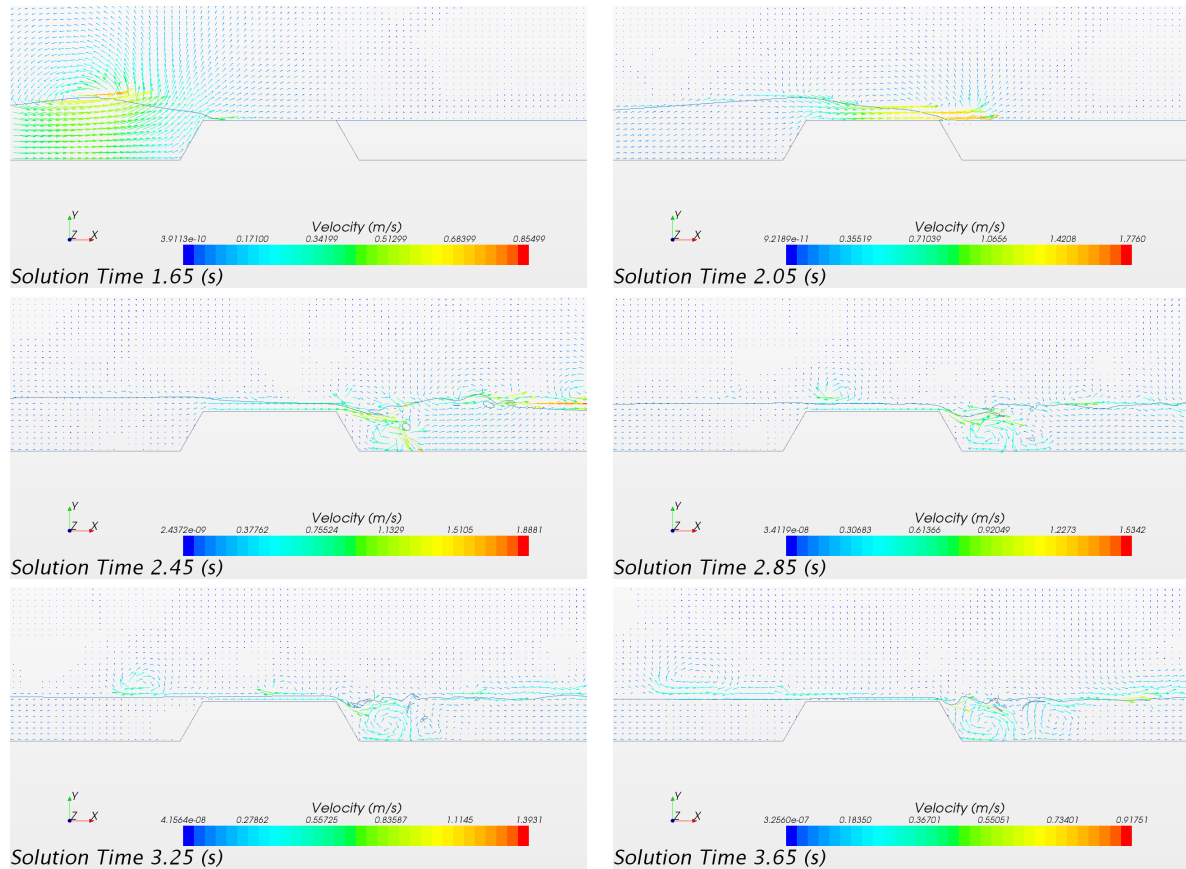


Figure 11: Computed velocity vector field at different time steps of vortex generation for solitary wave overtopping breakwater B ($H/d= 0.3$, $d = 22.86$ cm).

It is difficult to compare the performance of the standard K-Epsilon and SST-K-Omega models in terms of accuracy for water particle velocity at point E because their prediction accuracy changes for different sections of the plot. Also the quality of the experimental data, which is not as good as experimental data for the submerged break water case, is another reason that makes comparison of these turbulence models very difficult. Figures 10(c) and 10(d) present horizontal and vertical components of the water particle velocity at location F ($x = 2.22d$, $y = -0.5d$), which is in the same vertical line with location E but 0.4 depth lower. Comparing figures 10(a) and 10(c), it is observed that when the wave is propagating across this vertical line, the horizontal velocity at location E is in the shoreward direction (positive), whereas at location F it is in the seaward direction (negative). This is indicative of rotational motion of particles in the shoreward vicinity of the breakwater. Thus, the overtopping wave induces a complex rotational velocity field which is quite similar to that found in backward facing step flow except that the present flow condition involves an unsteady flow condition with a free surface. From figure 10(c) it can be seen that both standard K-Epsilon and SST-K-Omega models fail to predict the peak horizontal velocity at point F with reasonable accuracy. The same thing happens for vertical velocity at point F shown in figure 10(d), as both standard K-Epsilon and SST-K-Omega models significantly underpredict the magnitude of maximum vertical velocity at this point. Comparison of the simulation results of standard K-Epsilon and SST-K-Omega models to the experimental data for horizontal and vertical velocities at point F shows that both of these models perform similarly at this specific point and there is no clear advantage between the two turbulence models. Figures 10(e) through 10(h) show the comparison between first order and second order SST-K-Omega model simulations and the experimental data. The second order SST-K-Omega model seems to predict both horizontal and vertical velocity magnitudes at point E with slightly better accuracy than the first order SST-K-Omega model. Although the second order SST-K-Omega model slightly overpredicts the

magnitude of maximum vertical velocity at point E, it predicts the rest of horizontal and vertical velocity time histories with better accuracy. The advantage of the second order SST-K-Omega model over the first order SST-K-Omega model is more pronounced at point F. As is evident in figures 10(g) and 10(h), the second order SST-K-Omega model does a much better job of predicting the maximum and minimum horizontal and vertical velocity magnitudes. Although, especially for horizontal velocity, the second order SST-K-Omega model simulation results do not overlap the experimental data, the second order SST-K-Omega model seems to at least be able to predict the magnitude of minimum horizontal velocity with good accuracy. The same happens for vertical velocity, as again the second order SST-K-Omega model results are closer to the experimental data compared to the first order SST-K-Omega model. Zhuang and Lee (1996) reported this sequence of the vortex motion in the experiments with different breakwater height/water depth ratios. When the advancing wave propagated further toward the shoreward region the generated vortices moved downstream and were disintegrated eventually. Such kinematic properties have a direct impact on the stability of the breakwater units. Especially, as can be seen from Figure 11, a relatively large upward vertical velocity is generated near the shoreward region of the breakwater, which could cause a lifting force on the breakwater armor units in the shoreward side of the breakwater.

CONCLUSION

CFD simulations of transient nonlinear waves (modeled by solitary waves with moderate wave height) overtopping on coastal structures, such as breakwaters, have been conducted numerically. Based on the comparison of the numerical results to the experimental data, the following major conclusions for this study can be summarized:

1. CFD software was capable of capturing vortices that were generated in the vicinity of the shoreward region of breakwater and were captured experimentally as the solitary wave propagated over the top of the breakwater. CFD simulation results showed vortices which first stayed close to the shoreward breakwater surface and then moved downstream and were disintegrated eventually. Also, there was no apparent vortex motion observed in the simulation results at the seaward side of the breakwater when the solitary wave overtopped submerged breakwater, suggesting that the shoreward side of breakwater was more vulnerable than the seaward side. In addition, large horizontal velocities were observed in the shoreward region of the breakwater. This large horizontal velocity witnessed at the bottom of simulation domain could cause significant bottom scouring.
2. In the case of a solitary wave interaction with the breakwater which was at the same height as the still water, both the experimental data and the CFD simulation results show that a series of higher frequency oscillatory tails were generated in the shoreward region. This transmitted wave was then reformed to become a series of well-defined oscillatory waves as they propagate further away from the breakwater. This physical phenomenon is significant for the assessment of basin response of the shoreward coastal region. In addition, when the incident solitary wave overtopped the breakwater, both the experimental and CFD simulation results showed that the horizontal water particle velocity was nearly as large as the wave celerity. This indicates that the wave motion is transformed temporarily into a bore-like flow by the breakwater in the local area. The large horizontal and vertical velocities associated with an overtopping wave could produce significant impact on the marine structure located on the passageway of the overtopping waves.
3. CFD software was able to predict water surface profile and water particle velocities at the vicinity of the submerged breakwater with excellent accuracy. CFD simulations conducted using standard K-Epsilon, SST-K-Omega and inviscid models did not show any significant difference in submerged breakwater case. Standard K-Epsilon and SST-K-Omega models predicted water particle velocities at the vicinity of the breakwater with slightly better accuracy compared to the inviscid model, suggesting that the turbulence modeling does not improve the CFD simulation results drastically, and therefore extra computational costs associated with these kinds of CFD simulations might not be justified for this specific case.
4. CFD simulations conducted using standard K-Epsilon and SST-K-Omega models were able to predict water surface profile and water particle velocities at the vicinity of the breakwater with zero freeboard with reasonable accuracy. They were able to predict water surface elevations of both the solitary wave

and the reflected wave from the breakwater with excellent accuracy. However, while they were able to predict the maximum water surface elevations downstream of the breakwater, they failed to predict both the magnitude and the period of the oscillatory wave train at points located downstream of the breakwater with reasonable accuracy. CFD simulations of water surface elevations as well as oscillation period conducted using the second order SST-K-Omega model were better than the first order SST-K-Omega model, especially further downstream of the breakwater. The second order SST-K-Omega model was able to predict both the amplitude and the period of the oscillatory wave train with reasonable accuracy.

5. CFD simulations conducted using standard K-Epsilon and SST-K-Omega models were not able to predict the water particle velocities downstream of the breakwater with zero freeboard with reasonable accuracy, especially closer to the bottom boundary of the simulation domain. The second order SST-K-Omega model was able to predict the magnitude of the maximum horizontal and vertical water particle velocities with much better accuracy compared to the first order SST-K-Omega model.

References

- Mehrdad Bozorgnia and Jiin-Jen Lee. Computational fluid dynamic analysis of highway bridges exposed to hurricane waves. *Coastal Engineering Proceedings*, 1(33), 2012. URL <http://journals.tdl.org/icce/index.php/icce/article/view/6723>.
- Mehrdad Bozorgnia and Jiin-Jen Lee. Wave structure interaction during hurricane ivan simulated by a two-phase flow model. *Coastal Hazards*, pages 33–44, 2013. doi: 10.1061/9780784412664.004.
- Mehrdad Bozorgnia, Jiin-Jen Lee, and Frederic Raichlen. Wave structure interaction: Role of entrapped air on wave impact and uplift forces. *Coastal Engineering Proceedings*, 1(32), 2011. URL <http://journals.tdl.org/icce/index.php/icce/article/view/1358>.
- CD-adapco. User guide for star-ccm+ version 5.06.010. 2010.
- Ferziger, H. Joel, and Milovan Peric. *Computational Methods for Fluid Dynamics*. Springer-Verlag, Berlin, 2002.
- C.W. Hirt and B.D. Nichols. Volume of fluid (vof) method for the dynamics of free boundaries. *Comput. Phys.*, pages 201–225, 1981.
- W.P Jones and B.E Launder. The prediction of laminarization with a two-equation model of turbulence. *International Journal of Heat and Mass Transfer*, 15(2):301–314, February 1972. ISSN 00179310. doi: 10.1016/0017-9310(72)90076-2. URL <http://linkinghub.elsevier.com/retrieve/pii/0017931072900762>.
- B.E. Launder and B.I. Sharma. Application of the energy-dissipation model of turbulence to the calculation of flow near a spinning disc. *Letters in Heat and Mass Transfer*, 1(2):131–137, November 1974. ISSN 00944548. doi: 10.1016/0094-4548(74)90150-7. URL <http://www.sciencedirect.com/science/article/pii/0094454874901507>.
- Inigo J. Losada, Javier L. Lara, Raul Guanche, and Jose M. Gonzalez-Ondina. Numerical analysis of wave overtopping of rubble mound breakwaters. *Coastal Engineering*, 55(1):47–62, January 2008. ISSN 03783839. doi: 10.1016/j.coastaleng.2007.06.003. URL <http://linkinghub.elsevier.com/retrieve/pii/S0378383907000713>.
- S. Mozaferija and M. Peric. Computation of free surface flows using interface-tracking and interface-capturing methods. *Computational Mechanics Publications*, chap 2, 1998.
- Fredric Raichlen, Jack C. Cox, and Jerald D. Ramsden. Inner Harbor Wave Conditions due to Breakwater Overtopping. In *Coastal Engineering Practice (1992)*, pages 425–446. ASCE, 1992. URL <http://cedb.asce.org/cgi/wwwdisplay.cgi?75180>.
- F Zhuang and JJ Lee. A viscous rotational model for wave overtopping over marine structure. *Coastal Engineering Proceedings*, pages 2178–2191, 1996. URL <http://journals.tdl.org/icce/index.php/icce/article/viewArticle/5373>.